Low and high gamma oscillations deviate in opposite directions from zero-phase synchrony in the limbic corticostriatal loop

Authors: Julien Catanese[1], J. Eric Carmichael[1,2] and Matthijs A. A. van der Meer[1,2*]

[1]Department of Biology and Centre for Theoretical Neuroscience, University of Waterloo, Ontario, Canada

[2]Department of Psychological and Brain Sciences, Dartmouth College, USA

[*]Correspondence should be addressed to MvdM. Current address: Department of Psychological and Brain Sciences, Dartmouth College, Hanover, NH 03755. E-mail: mvdm@dartmouth.edu.

Running head: Low and high gamma directionality

Keywords: accumbens, prefrontal cortex, synchrony, phase-slope index, cell assembly, neural ensemble

Number of Figures: 9

Abstract

The loop structure of cortico-striatal anatomy in principle enables both descending (cortico-striatal) and ascending (striato-cortical) influences, but the factors that regulate the flow of information in these loops are not known. We report that low- and high-gamma oscillations ($\sim$50Hz and $\sim$80Hz respectively) in the local field potential of freely moving rats are highly synchronous between the infralimbic region of the medial prefrontal cortex (mPFC) and the ventral striatum (vStr). Strikingly, high-gamma oscillations in mPFC preceded those in vStr, whereas low-gamma oscillations in mPFC lagged those in vStr, with short ($\sim$1ms) time lags. These systematic deviations from zero-phase synchrony were consistent across measures based on amplitude cross-correlation and phase slopes, and were robustly maintained between behavioral states and different individual subjects. Furthermore, low- and high-gamma oscillations were associated with distinct ensemble spiking patterns in vStr, even when controlling for overt behavioral differences and slow changes in neural activity. These results imply that neural activity in vStr and mPFC is tightly coupled at the gamma timescale, and raise the intriguing possibility that frequency-specific deviations from this coupling may signal transient leader-follower switches.

Introduction

The parallel loops that recurrently interconnect the cortex, basal ganglia, and thalamus are a major structural feature of the mammalian nervous system, generally thought to be broadly involved in the selection, initiation, and refinement of actions across domains from motor to cognitive (Alexander and Crutcher, 1990; Pennartz et al., 2009; Humphries and Prescott, 2010). In each loop, the signal flows from cortex to striatumm, through other basal ganglia nuclei, and out through the thalamus back to cortex. However, within these loops there are back-projections, and particularly in the limbic loop that includes prefrontal cortex and the ventral striatum, nodes receive input from other brain areas such as the hippocampus and amygdala (Haber et al., 2000; Voorn et al., 2004). The question thus arises how the flow of information is controlled in this architecture: for instance, are the nodes that form a loop always coupled, or can one transiently become a "leader" while others follow?

One approach for addressing this issue is though examination of oscillations in local field potentials (LFPs), which are thought to reflect temporal organization in meso-scale neural activity arising primarily from summed synaptic currents (Mitzdorf, 1985; Nunez and Srinivasan, 2006; Buzsáki et al., 2012). Influential proposals such as "communication through coherence" and its relatives ("CTC"; Singer 1999; Fries 2005) suggest that effective connectivity between networks and brain structures can be modulated at fine timescales by the degree of coherence (synchrony) between oscillations in participating regions. This notion has found substantial modeling and experimental support in a variety of neural systems and rhythms (Akam and Kullmann 2014; Bosman et al. 2012; Lisman and Jensen 2013; although is not free of pitfalls, see e.g. Buzsáki and Schomburg 2015), raising the possibility that neural synchrony reflected in LFP oscillations may also contribute to regulating the flow of information in cortico-striatal loops.

Even in the absence of postulating a mechanistic role for LFP oscillations in such routing or gain control, such oscillations can serve as markers that provide information about the spatial and temporal organization of neural activity within and across brain regions (Friston et al., 2014). In the corticostriatal network specif-

ically, LFP activity is known to change with learning (Howe et al., 2011; Koralek et al., 2013; Thorn and Graybiel, 2014) and different behavioral states (Berke, 2009; Gruber et al., 2009; Leventhal et al., 2012), and serves as a biomarker of behavioral and neurological disorders in humans (Boraud et al., 2002; Hammond et al., 2007) and animal models (Courtemanche et al., 2003; Cruz et al., 2011; Lemaire et al., 2012; Dejean et al., 2012). Importantly, a number of studies have shown that spike timing is systematically related to these oscillations (Berke et al., 2004; Sharott et al., 2009; Howe et al., 2011) demonstrating that although the sources of the LFP oscillations in the basal ganglia may not yet be completely clear, they contain information about local spiking activity.

Here we focus on gamma oscillations, which are prominent in prefrontal cortex, ventral striatum, and other nodes of the limbic system (van der Meer et al., 2010; Dejean et al., 2011; Stujenske et al., 2014; Donnelly et al., 2014) and therefore provide a potential access point for determining how the temporal dynamics of neural activity across this network are organized. Classically, gamma oscillations are thought of as a relatively local phenomenon, generated by the interplay of fast excitatory-inhibitory feedback loops (Bartos et al., 2007; Buzsáki and Wang, 2012; Womelsdorf et al., 2014). However, observations and computational models of long-range gamma synchrony in the face of significant conduction delays (Traub et al., 1996; Gollo et al., 2014) have shown that even distant regions can exhibit coordinated activity in this frequency range, potentially playing a role in binding, gain control or routing, and plasticity (Fries et al., 2007; Uhlhaas et al., 2009; Bastos et al., 2015).

Specifically, by recording simultaneously in mPFC and vStr, we show that gamma oscillations in these regions are strongly synchronized. Strikingly, amplitude and phase lags between the two sites were very close to zero, as in the classic long-range zero phase lag results (Traub et al., 1996; Buzsáki and Schomburg, 2015), but also suggestive of volume conduction from a common source. However, closer examination revealed that low- and high-gamma frequencies, previously shown to have different relationships to behavior, learning and spiking activity (van der Meer and Redish, 2009b) were in fact associated with systematic deviations from zero phase lag, in opposite directions. Furthermore, these oscillations were associated with distinct neural

ensembles, as shown with a multivariate classifier.

Materials and Methods

Subjects and overall timeline. This study consists of two experiments, performed on different sets of subjects. Experiment 1 centers on the relationship between mPFC and vStr gamma oscillations in the local field potential (LFP), performed on a new (previously unpublished) data set described in detail here. Experiment 2 relates vStr gamma oscillations to ensemble spiking patterns. Because this latter experiment uses a previously described dataset (van der Meer and Redish, 2009a,b) the experimental procedures are not repeated here; only analysis sections "Gamma event detection" and "Ensemble classification" apply to these data.

Subjects for the mPFC-vStr LFP study (Experiment 1) were four male Long-Evans rats (Harlan, Mississauga), 4-5 months old at the start of training and food-restricted to no less than 85% of their maximum pre-training weight. All animals were housed on a 12 hr:12 hr light/dark cycle, with experiments performed during the light phase.

Rats were first familiarized with the experimental environment by daily handling in the experimental room and free exploration of the experimental apparatus for 5 days. Next, rats were trained to shuttle back and forth along a linear track, described below, until a criterion of 100 trials in a 40-minute session was reached (this took 6 ± 2 days, mean $\pm$ SD). Rats were given two days of full rest with ad-libitum food before surgery. After surgery rats were allowed to recover for at least 5 days (mean: 8 ± 2 days), before any further training. Before neural recording commenced, rats were retrained for 7 ± 3 days until they again reached the performance criterion of 100 trials per 40 minutes.

All procedures were pre-approved by the Animal Care Committee of the University of Waterloo (AUPP

11-06) and in accordance with Canadian Council for Animal Care (CCAC) guidelines.

Behavioral task. The apparatus for Experiment 1 was a 184-cm long elevated linear track (Figure 1A, one run is defined as a trial). Rats could nosepoke into photobeam-equipped receptacles for food reward (two TestDiet 5TUL 45 mg pellets at each end). Reward delivery was triggered following a 700 ms nosepoke into the reward receptacle, with a further 800 ms or more required for pellets released from the pellet dispensers (Coulbourn) to reach the rat. The basic linear track configuration was a "no-choice" task (Figure 1A, left) in contrast with the "one-choice" version of the task (Figure 1A, right; see caption for details) which was started once rats completed 7 recording days on the "no-choice" task. Track configurations (direction of the 45-degree ends, and location of the Y-piece) were pseudorandomized across days. The analyses and results reported collapse across the two task versions, since no differences were apparent at the neurophysiological level.

[Figure 1 about here.]

Electrode arrays and surgery. Rats were chronically implanted with a total of twelve independently movable electrodes (stereotrodes or tetrodes): four in the ventral striatum (AP +1.3-1.7mm and ML +1.6-2.4mm relative to bregma), two in the medial prefrontal cortex (AP +3mm and ML +0.6mm), two in the amygdala (AP -2.2mm and ML +5.3mm), four in the ventral hippocampus (AP -4.9mm and ML +5mm; all targets on the right hemisphere). Because ventral hippocampal and amygdala electrodes did not reliably reach their intended targets, only recording data from vStr and mPFC were analyzed here.

Surgical procedures were as described previously (Malhotra et al., 2015). Briefly, rats were deeply anesthetized, initiated by pentobarbital injection (50mg/kg i.p.) and maintained by isoflurane inhalation (0.5-2% in 0.7-1 l/min oxygen). Following administration of an analgesic (Anafen, 10 mg/kg s.c.) and antibiotic (Duplo-cillin, i.m.) the scalp was shaved and disinfected before exposing the skull surface, into which jewelers' screws were inserted and craniotomies were drilled. Dura was removed before the electrode bundle

was lowered to the cortical surface. The implant was secured to the skull with dental acrylic (Jet Acrylic, Lang Dental Co. and Metabond, Parkell) and a ground connection made to a skull screw on the contralateral parietal bone. Following surgery, rats were given at least 5 days to recover before behavioral training recommenced.

Neural data acquisition. Tetrodes and stereotrodes made from 17μm platinum-iridium, teflon-coated wire (California Fine Wire) were plated with platinum black solution to 200-400kΩ impedance (measured at 1kHz, BAK-1 impedance tester, BAK Electronics), assembled into independently movable bundles as described previously (Malhotra et al., 2015), and soldered to a Neuralynx EIB-36-16TT interface board. LFPs were acquired at 2kHz using a Neuralynx preamplifier (HS-36) and data acquisition system (Digital Lynx SX). Importantly, a panel ground reference was used for all recordings to avoid contamination from a common neural reference.

Recording of synthetic test signals. To test if filtering at the data acquisition and processing stages, and/or differences in electrode impedance could account for the observed results, we recorded synthetic signals from a signal generator (Minirator MR2, NTi). Using a Buzsaki32L probe (NeuroNexus B-stock) consisting of four 8-site shanks with 32 total recording sites (of which 24 were functional), we first determined the impedance of each recording site (NanoZ, Multi Channel Systems; measured at 1kHz and 100Hz). Next, we recorded 40, 63, 80 and 100Hz signals of 100 μV each in amplitude by placing the probe in a 0.9% saline solution connected to the signal generator; thus, all sites are presented with an identical test signal. We then analyzed the phase lag between signals recorded from each pair or recording sites as a function of frequency and impedance to determine (1) if any systematic deviations from the theoretical zero phase lag resulted, and (2) compare these deviations to those observed in the neural data.

Experimental control. A custom-written MATLAB script accessed video tracking data and photobeam status through the NetCom interface and software (Neuralynx), such that rewards could be delivered according to the task design.

Histology. After data collection was complete, 10μA current was passed through the electrodes for 10s each. One rat did not undergo this gliosis procedure because of premature detachment of the electrode array. Three days following gliosis, rats were anesthetized with isoflurane, asphyxiated and perfused intracardially with 10% formalin. Brains were extracted and stored in formalin with 30% sucrose before being cut in 50μm sections using a freezing microtome. Sections were mounted on gelatin-coated slides, stained with metachromatic thionin and coverslipped for localization of recording locations. Only data from electrodes with confirmed recording locations in vStr and the infralimbic area of the mPFC were analyzed (Figure 2).

Analysis overview. All analyses were performed using MATLAB R2014a, and can be reproduced using code on our public GitHub repository (`https://github.com/mvdm/papers/Catanese_vanderMeer2016/`). Original data files, metadata, and codebase tutorials will be provided on request.

For Experiment 1 (Figures 3-6), local field potentials (LFPs) were recorded from vStr and the infralimbic region of the mPFC. Two sessions per rat were analyzed. For each rat, we selected the session from the no-choice task and the one-choice task with the highest number of trials (except for Rat 3, for which 2 sessions from the no-choice task were selected because no data were available from the one-choice task). The results obtained in the two task conditions were similar, therefore analyses collapsed across tasks (no-choice and choice) and across reversals in the choice version of the task.

For Experiment 2 (Figures 8-9), LFPs and spike waveforms were recorded from the vStr only, as described in van der Meer and Redish (2009b). All recording sessions with at least 25 simultaneously recorded neurons were included, for a total of 64 sessions from 4 animals.

Data pre-processing (both experiments). Because neural signals for Experiment 1 were recorded against ground (rather than a skull screw or intracranial reference), removal of mechanical artifacts in the data was required. All intervals exceeding a threshold (+/- 750μV), plus 100ms either side, were detected as an artifact and eliminated from analysis.

Next, to detect and eliminate contamination from muscle activity, such as occurs during chewing, LFPs were band-pass filtered between 125-250Hz (this EMG frequency band was determined by visual inspection of spectrograms). Intervals with an amplitude envelope greater than one standard deviation (Experiment 1) or 1.5 standard deviations (Experiment 2) from the mean, plus 100ms on either side, were considered chewing events and eliminated from further analysis. (Different thresholds were used because in Experiment 1, data were recorded against ground, whereas those in Experiment 2 were recorded against a reference electrode located in the overlying corpus callosum.) Note also that data analyzed during task performance, when chewing was most likely to occur (reward epoch; Figure 1a), were restricted to a window of 0 to 1.5s following the nosepoke, before contact with reward pellets is made.

Finally, we found that gamma events could sometimes be partially overlapping with spindle oscillations or K-complex like waveforms, associated with transient 25-30Hz power. To avoid potential gamma contamination by these events, LFPs were band-pass filtered between 25 and 30Hz to detect and remove these events; intervals with a power greater than one standard deviation from the mean, plus 100ms either side, were considered as "K-like" event and removed from analysis.

Analysis epoch definition (Experiment 1). Analyses were performed on the full task session, on off-task rest, or on specific task epochs ("Run" and "Reward"), as indicated in the main text. For Run, session data was restricted to on-task times when animals moved at a speed of $\sim$10 cm/s or more. For Reward, data was restricted to the pre-reward nosepoke period (0 to 1.5s relative to nosepoke initiation; food pellets do not reach the animal until after 1.5s). "Rest" refers to data acquired while animals rested in their home cage following task completion.

Spectral Analysis (Experiment 1). We first characterized the overall spectral properties of vStr and mPFC LFPs over a broad frequency spectrum for the entire recording session, as well as for specific epochs ("Rest", "Run", "Reward"). Power spectral densities (PSDs) were computed with the MATLAB `pwelch()` function and normalized by $1/f^2$; coherence was computed with `mscohere()`, both using a 1-second Hanning

window with 50% overlap.

Gamma event detection (both experiments). Next, we focused on gamma-band oscillations by detecting transient events during which the gamma-band envelope exceeded a significance threshold (Figure 1B). This detection was performed on the vStr LFPs because the amplitude of gamma events systematically exceeded that of synchronous events recorded in mPFC (Figure 2B and 3). For this purpose, LFPs were first filtered in the low-gamma (45-65Hz) or high-gamma band (70-90Hz) using a 5th order Chebyshev filter (passband ripple, 0.5 dB) and the MATLAB `filtfilt()` function. Instantaneous signal amplitude was obtained by taking the modulus of the Hilbert-transformed signal (MATLAB `abs(hilbert())`). Gamma events were detected when this amplitude envelope exceeded the 95th percentile of the amplitude distribution (across the entire session), and contained at least three oscillation cycles of at least 50μV in amplitude. Events separated by 50ms or less were merged (if both were of the same gamma type) or excluded (if different gamma type). All gamma-specific analyses were applied to 400ms windows centered on these events.

Amplitude cross-correlations (Experiment 1). To determine the temporal relationship between vStr and mPFC LFPs, we first employed an event-based version of the cross-correlation analysis in Adhikari et al. (2010). We obtained gamma-band envelopes for both LFPs as described above, and for each gamma event separately, found the peak of the cross-correlation (from -50 to +50ms, MATLAB `xcov()` function) computed on the rank-transformed envelopes. We then tested if the distribution of peak locations was significantly shifted from zero, for the set of low- and high-gamma events separately (one-sample Wilcoxon ranksum test) and if the distribution of cross-correlation peaks was different between low- and high-gamma events (two-sample Wilcoxon ranksum test). To ensure that cross-correlations were computed on gamma events that were present in both mPFC and vStr, the peak cross-correlation for each event was required to pass a permutation test in which the phases of the Fourier transform were randomly reassigned. Only events in which the peak cross-correlation was in the top 5% relative to 1000 such permutations were used in the cross-correlation analysis.

Phase slopes and phase-slope index (PSI, Experiment 1). Next, we computed the phase-slope index (PSI, Nolte et al. 2008) using the FieldTrip toolbox (Oostenveld et al., 2011), a measure that quantifies the dependence of phase lag on frequency (Figure 5a). To this end, we first computed the phase lag (angle of the coherency) between vStr and mPFC LFPs across the frequency spectrum (from 40 to 120 Hz, in steps of 1Hz) using a multitaper method (FieldTrip `ft_freqanalysis()`, `mtmfft` method with `tapsmofrq` set to 4). These parameters were chosen because they performed best in recovering ground truth time lags in simulated data; changing the level of frequency smoothing (`tapsmofrq` = 8, or to a single Hanning window) resulted in minor numerical differences, but did not change the pattern of results. After verifying that these phase cross-spectra contained linear regions (phase slopes; example phase spectra are shown in Figure 5b and 6a) we computed the phase-slope index using the FieldTrip `ft_connectivity()` function with bandwidth 4.

To infer the time lag (or lead) between vStr and mPFC from observed phase slopes, we used the following equation:

$$t_{a-b} = [\frac{\phi_{a-b}(f+df) - \phi_{a-b}(f)}{df}]/360^\circ \quad (1)$$

where t_{a-b} is the time lag (or lead) in seconds between signals a and b, to be inferred from the phase differences ϕ_{a-b} (in degrees) observed at frequencies f and $f + df$. For instance, given a phase difference $\phi_{a-b} = 45^\circ$ between signals a and b at $f = 25$Hz, and $\phi_{a-b} = 36^\circ$ at $f = 20$Hz, $t_{a-b} = [(45 - 36)/(25 - 20)]/360 = 5$ms (Figure 5a). As $df \to 0$, the fraction shown in square brackets above corresponds to the derivative $\phi'_{a-b}(f)$, i.e. the phase slope. Positive time lags indicate that a leads b.

Ensemble classification (Experiment 2). For the results in Figure 9, we analyzed data from a previously published dataset (van der Meer and Redish, 2009a,b) in which electrodes were located in the vStr only in order to maximize the number of simultaneously recorded units. Experimental procedures for these data were

similar to those described for Experiment 1, except that the task used was a modified T-maze instead of a linear track (van der Meer and Redish, 2009a). Gamma events were detected with the same parameters as for Experiment 1, described above, with the exception that no absolute amplitude threshold was used (because LFPs in this data were recorded relative to an intracranial reference, signal amplitudes were generally lower and this threshold was unnecessary). To minimize the impact of overt behavioral differences, only gamma events that occurred off-task (on a terracotta pedestal filled with towels) or at a single reward site on the task ("Feeder 2", van der Meer and Redish 2009a) were included.

To probe the relationship between gamma events and spiking activity, we first converted spike rasters obtained from simultaneously recorded vStr neurons into vectors of spike counts (one N x 1 vector for each gamma event, where N is the number of neurons in the data set), normalized to firing rates. Using 10-fold cross-validation, we trained a linear discriminant classifier (MATLAB `classify()` function) to classify these spike count vectors as low-gamma or high-gamma (Figure 8). In increments of 5 cells, we sampled randomly from the total number of neurons in the recorded ensemble (1000 samples per ensemble size) and obtained the classification performance of the best performing ensemble. Thus, classification performance of ensemble size 1 indicates the performance of the single best neuron; classification performance at ensemble size 6 indicates the performance of whichever subset of 6 neurons performed best, and so on.

Because different sessions had different numbers of detected low- and high-gamma events, we subsampled from the frequency band with the largest number of events, ensuring that chance performance was at 50% for each session. As a control, we performed the same analysis on a set of spike count vectors with the spike data shifted up to 5s relative to the LFP. The exact time shift was determined on an event-by-event basis by finding the time with the lowest broadband gamma power (40-100 Hz) within 5s either way from each actual event.

We tested a number of different classifiers in addition to the linear discriminant, and found that Naive Bayes, k-nearest-neighbor (with k = 9; other values of k were worse) and a support vector machine (MATLAB

`svmclassify()`) all returned relatively similar performance. Thus, we report only the linear discriminant results here.

[Figure 2 about here.]

Results

Experiment 1

We recorded local field potentials (LFPs) simultaneously from the infralimbic region of the medial prefrontal cortex (mPFC) and ventral striatum (vStr) from four rats running linear tracks for food reward (Figure 1A). Rats ran an average of 124 $\pm$ 27 (mean $\pm$ S.E.M) trials per 40-minute session. Each task session was immediately followed by a rest session consisting of a 40-minute home cage recording. All recordings were referenced against recording system ground to avoid spurious correlations due to a common reference signal.

As reported previously, vStr and mPFC both exhibited LFP oscillations in the gamma band, with distinct oscillations in the low-gamma (45-65Hz) and high-gamma (70-90Hz) bands that manifest as transient "events" (Figure 1B; van der Meer and Redish 2009b; Berke 2009; Howe et al. 2011; Dejean et al. 2013). These two gamma bands appear as elevated regions in the power spectrum densities for both mPFC and vStr regions (Figure 3A; mean over task sessions). As in our previous reports investigating the behavioral correlates of vStr gamma (Malhotra et al., 2015; van der Meer and Redish, 2009b), the vast majority of low- and high-gamma occurred when the animal is stationary, such as occurs at the reward sites on the task, and during off-task rest periods. When gamma events occurred, low- and high-gamma oscillations tended to follow a characteristic fine-timescale alternating pattern in which low-gamma leads high-gamma (Malhotra et al., 2015). Other groups have reported similar properties, as well as further behavioral correlates and dissocia-

tions between the two gamma bands (Kalenscher et al., 2010; Howe et al., 2011; Morra et al., 2012; Donnelly et al., 2014). Experiment 1 focused on the relationship between gamma oscillations in the vStr and mPFC.

Gamma oscillations are synchronized in phase and amplitude between ventral striatum and medial prefrontal cortex

Visual inspection of raw LFP traces suggested a clear relationship between gamma oscillations in mPFC and vStr: gamma events in both traces tended to co-occur in time (Figure 1B). We quantified this relationship first by computing the correlation between the signal power of vStr and mPFC LFPs across frequencies (Figure 3B). The elevated correlation in the gamma band – including low and high gamma – indicates that power in the gamma band was more strongly correlated between structures than neighboring frequencies. Comparison of the observed correlation coefficients with a distribution of permuted correlations, obtained from 1000 samples in which one of the two power time series was circularly shifted by a random amount, indicated that the observed correlations were reliably larger than this permuted distribution for both low- and high-gamma ($p < 10^{-3}$).

[Figure 3 about here.]

Second, to capture the phase relationship between gamma in mPFC and vStr, we computed the coherence spectrum, which quantifies the phase consistency between signals (Figure 3C). This similarly revealed elevated coherence in the gamma band, including both low and high gamma. To characterize how gamma oscillations were modulated by behavior, we repeated the same set of analyses on three different behavioral epochs: "run"; "reward" and "rest" (see *Materials and Methods*). All three epochs exhibited power in the gamma band (Figure 3D), and both amplitude (Figure 3E) and phase (Figure 3F) relationships between vStr and mPFC were preserved. As expected from our previous report (Malhotra et al., 2015), gamma power was highest during rest, and the lowest during run, while theta power (7-10 Hz) showed the opposite pattern.

Furthermore, during run, the gamma power peak was shifted toward higher frequencies, as has been found in the dorsal striatum (von Nicolai et al., 2014). Taken together, these results indicate that despite these state-dependent changes, gamma amplitude and phase relationships were essentially unaffected.

High and low gamma oscillations are associated with distinct directionality through the cortico-striatal loop

Amplitude and phase correlations can establish that mPFC and vStr gamma are related, but cannot determine if one leads or lags the other. To address directionality, we used two different methods that rely on amplitude and phase respectively: cross-correlation of gamma amplitude in time (Adhikari et al., 2010), and the phase-slope index (PSI, Nolte et al. 2008); for both, we first detected gamma events using an amplitude threshold on the bandpass-filtered signal (low gamma: 45-65 Hz; high gamma: 70-90 Hz; see *Materials and Methods*). We detected and analyzed a total of 2733 low-gamma and 7390 high-gamma events (task: 456 low-gamma and 1908 high-gamma, 1.4 and 5.8 events/min respectively; rest: 2267 low-gamma and 5439 high-gamma, 4.6 and 11.0 events/min respectively).

To obtain an estimate of directionality based on the relative amplitudes of mPFC and vStr gamma, we detected the time shift for which their correlation was maximal, after excluding events in which there was no statistical evidence of a gamma amplitude cross-correlation (Figure 4A,B). The distribution of peak correlation times for high-gamma was significantly different from zero, indicating a mPFC lead (+0.59ms; $p = 6.98 * 10^{-15}$; one-sample Wilcoxon test). The low gamma distribution of peak correlation times was also significantly different from zero, but in the opposite direction, indicating a vStr lead (-0.30ms; $p = 1.26 * 10^{-2}$; one-sample Wilcoxon test). This asymmetry was visually apparent both from the average cross-correlation across all events (Figure 4A, top panel) and from the histograms of peak cross-correlation times (bottom panel; note arrows indicating increased vStr lead counts for low-gamma, and increased mPFC lead counts for high-gamma).

[Figure 4 about here.]

To obtain independent confirmation of the above pattern of results, we used the phase slope index (PSI, Nolte et al. 2008, as implemented in the FieldTrip toolbox; Oostenveld et al. 2011) which is based on the phase relationship between two signals (Figure 5). Specifically, if there is a constant time lag between two signals, as expected if a signal from one structure leads the other, then there is a linear relationship between phase lag and the frequency, whose slope indicates the sign and magnitude of the time lag (illustrated in Figure 5a). Crucially, we chose to use the PSI measure here because unlike typical autoregressive methods (e.g. Granger causality) PSI is relatively insensitive to false positives due to independent noise corrupting a common signal. In particular, since mPFC gamma tends to be lower amplitude than vStr gamma, Granger causality tends to identify vStr as Granger-causal to vStr even for zero time lag (as shown in Nolte et al. 2008 and the FieldTrip connectivity tutorial).

[Figure 5 about here.]

Starting with the raw phase slopes, obtained from the phase lag as a function of frequency (Figure 5B, top) we observed a slope sign inversion around 65-70 Hz, with a positive slope in the low gamma band and a negative slope in the high gamma band. This pattern indicates a vStr lead in the low gamma band, and a mPFC lead in the high gamma band (Figure 5B, middle). This phase slope reversal between low- and high gamma was consistent across individual subjects (Figure 6A) and clearly evident in the grand average mean phase slope index (Figure 6B). Consistent with this result, the mean phase lag between vStr and mPFC shifted systematically from a vStr lag in the low gamma band to a mPFC lead in the high-gamma band (Figure 6D-E). However, it is important to recognize that this measure is inherently circular, as well as sensitive to recording location relative to current sinks and sources (Nunez and Srinivasan, 2006; Buzsáki et al., 2012).

[Figure 6 about here.]

To test if this result was modulated by behavior, we compared the mean PSI and phase lag during rest and task (Figure 6C, E). A similar pattern of directionality was obtained, with a noticeable shift toward lower frequency during rest, consistent with the similar shift in the power spectra (Figure 3). Finally, in order to estimate the time lag/lead between mPFC and vStr for both gamma bands, we used the linear relationship between phase slope and time lag (Equation 1). Based on the grand average phase slope, we found that vStr leads mPFC in the low-gamma band by 1.3 ms, and mPFC leads vStr by 0.52 ms in the high-gamma band. Although these values do not exactly match those obtained from the amplitude cross-correlation method, the millisecond timescale and directionality reversal between low- and high-gamma are preserved across methods.

The relatively small, single-millisecond magnitude of the time lags we observed raise the possibility that some property of the recording electrodes and/or the recording system may be a factor. To test this possibility systematically, we recorded test signals in the 40-100Hz range (40, 60, 83 and 100 Hz sinusoids, 100 μV magnitude) simultaneously across 24 recording channels with a range of impedances (mean: 0.78MΩ, minimum: 0.58MΩ, maximum: 1.02MΩ). The phase lags and phase slopes we observed in this setting were about a factor 40 smaller than those experimentally (Figure 7; compare the neural data Figure 6). The synthetic phase lags showed some dependence on signal frequency (mean phase lag for 40 Hz: 0.0023°$\pm$ 0.12, 100 Hz: -0.0177°$\pm$ 0.15; ANOVA main effect, $F_{(3)}$ = 2.7, p = 0.047) and impedance (averaged over the two electrodes in the pair, ANOVA main effect, $F_{(226)}$ = 9.51, p $< 10^{-5}$). Crucially however, there was no evidence of an interaction between impedance and frequency (ANOVA $F_{(3,226)}$ = 0.07, n.s.). This pattern did not change when taking the absolute value of the phase lags (since the choice of pair order is arbitrary). Thus, the observed phase lags and reversal across low- and high-gamma frequencies cannot be explained by electrical or filtering properties of the recording setup.

[Figure 7 about here.]

Taken together, these results indicate that mPFC high gamma oscillations systematically lead the vStr by

about 0.5 ms, and vStr low gamma oscillations systematically lead those in mPFC by about 1 ms.

Experiment 2: High and low gamma oscillations are associated with distinct cell assemblies in the ventral striatum

A crucial indicator of the relevance of local field potential oscillations for information processing is the extent to which they are associated with spiking activity. Given the dissociation in directionality between low- and high-gamma observed in the previous section, we hypothesized that these two distinct gamma oscillations would also be associated with distinct cell assemblies in the ventral striatum. We test this idea in Experiment 2.

Specifically, we used a suite of classifiers that attempted to infer the identity (label) of the gamma oscillation ("low" or "high") based on the firing rates of ensembles of simultaneously recorded neurons. If it is possible to predict better than chance the label of the gamma event from the ensemble firing rates, this implies that there is a systematic relationship between the LFP and the information represented in the ensemble firing rates. Note that this approach tests for a very different relationship between LFP and spiking activity than measures such as spike-field coherence, which quantify entrainment or phase-locking of spiking to the LFP (Berke et al., 2004; van der Meer and Redish, 2009b; Howe et al., 2011), and generalizes our previous results examining single cells (van der Meer and Redish, 2009b). For this analysis, we used a different dataset (4 rats, 13-19 sessions per rat) containing large ensembles of vStr neurons recorded simultaneously along with LFPs as the rats ran a modified T-maze task (data set previously reported in van der Meer and Redish 2009a,b).

As in the directionality analysis above, high and low gamma events were first detected, and then associated with the corresponding vector of spiking activity (Figure 8A). Linear discriminant classifiers were trained to associate low-gamma and high-gamma class labels in the training data set with points in N-dimensional

space, corresponding to the (normalized) event spike counts for an ensemble of N neurons. Classifier performance was then measured by class label accuracy on spike count vectors in the testing set (withheld from training; 10-fold cross-validation with 100 iterations). The analysis was also repeated for a control condition in which spike counts were taken from a nearby time period of equivalent length, which did not correspond to a detected gamma event (see *Materials and Methods*).

[Figure 8 about here.]

The results (averaged over 64 sessions) show that the classifier performed significantly better than the control condition (Figure 8B; ANOVA main effect $F_{(1)}$ = 201.96, p $< 10^{-16}$). Furthermore, the error rate decreased as the number of neurons used was increased (ANOVA main effect $F_{(4)}$ = 40.16, p $< 10^{-16}$). This pattern of results was consistent across individual subjects (Figure 9). Note that this analysis necessarily underestimates the true performance of the best performing ensemble, due to the large numbers of possible "n-choose-k" subsets which are sampled from, rather than exhaustively tested, here. In any case, it is clear that low and high gamma oscillations in the local field potential are associated with distinct activity patterns in vStr neural ensembles.

[Figure 9 about here.]

Compared to our previous report of single vStr cells modulating their firing rates as a function of low- and/or high-gamma power (van der Meer and Redish, 2009b), the current analysis is improved in several ways. First, most obviously, it generalizes the issue to the ensemble level. Although the observation that the identity of the gamma event can be predicted from the ensemble is necessarily implied by the known single cell firing rate modulation, the ensemble classification permits quantification of the more biologically relevant issue of to what extent multiple cells contain redundant or synergistic information – by showing how classification performance improves as a function of the number of cells. It is also less *ad hoc*, putting the analysis in a common metric (classification performance) which can accommodate other sources of information in the

future.

In addition, the present analysis contains important controls, in that we (1) only used gamma events at "behaviorally clamped" locations, and (2) compared classification performance to a time-shifted control. Given the known different time courses of low- and high-gamma (van der Meer and Redish, 2009b; Howe et al., 2011) and the known ventral striatal single neuron tuning of e.g. "ramp" neurons, correlations between gamma power and firing rate could arise through independent alignment. These two controls reduce the possible contribution of overt behavioral differences and slow changes in unit activity which may correlate with gamma event occurrence.

Discussion

We have shown that low and high-gamma oscillations in the mPFC and vStr local field potential (LFP) are tightly synchronized, yet associated with opposite time lag/lead and distinct spiking activity patterns in vStr. Gamma-band synchrony between these structures has been noted or implied in previous studies (Berke 2009; Dejean et al. 2013; Donnelly et al. 2014 in rats, Cohen et al. 2012 in humans) but not analyzed in detail. In particular, previous work has been limited to analyses of coherence, which does not address the issue of directionality. Here, we show that mPFC leads vStr during high-gamma, but vStr leads mPFC during low-gamma LFP oscillations. Importantly, this pattern was consistent across subjects, as well as across distinct analysis methods that rely on independent features of the LFP (phase-slope index for phase, and cross-correlation for amplitude), and could not be accounted for based on electrode or recording system properties. In addition, we apply an ensemble classification method for quantifying the relationship between LFP and spiking activity to demonstrate, in a robust and generalizable manner, that low- and high-gamma activity in this circuit are associated with distinct local spiking.

Possible explanations for the mechanisms of gamma synchronization between mPFC and vStr

How should this striking temporal pattern of gamma oscillations in mPFC and vStr be interpreted? Near-zero phase lag synchrony in the gamma frequency band between anatomically separated areas has been reported in a number of different brain networks, such as between cortical areas (Traub et al., 1996) and between prefrontal cortex and the amygdala (Likhtik et al., 2014). At first glance, it may seem surprising that such fast oscillations, with cycle times in the range of 10-25 ms, can synchronize despite significant conduction and synaptic delays. However, mathematical analysis and computational modeling studies have shown that even relatively weak and slow long-range anatomical connections, in principle, are sufficient for such synchronization (Traub et al., 1996; Buzsáki, 2006; Vicente et al., 2008; Gollo et al., 2014). In the classic "coupled oscillator" models, the synchronizing elements are reciprocally (symmetrically) coupled, a scenario which is only approximately applicable to the mPFC-vStr circuit: although mPFC projects directly to vStr, the back-projection from vStr to mPFC is indirect, through the pallidum and thalamus (Haber, 2009; Sesack and Grace, 2010). How this specific degree of asymmetry in the mPFC/vStr coupling is expected to affect LFP synchrony is a question that can be addressed with computational models.

In any case, the possible interpretation that mPFC-vStr synchrony reflects the coupling of oscillators requires ruling out a number of alternative explanations (Buzsáki and Schomburg, 2015). Looming large among these is the possibility of a common source, whether volume-conducted or synaptically driving. Although a recent computational model found such a scenario, surprisingly, to be less robust than coupling for generating zero-lag synchrony (Gollo et al., 2014), there are several prominent common sources to consider. First, the piriform cortex is located close to both mPFC and vStr, with a recent study demonstrating vStr gamma oscillations in the LFP are dominated by a piriform source (Carmichael and van der Meer, 2015). Further possibilities for common sources include the intermediate to ventral hippocampus, which projects monosynaptically to both vStr and mPFC (Jay and Witter, 1991; Groenewegen et al., 1987), and generates low and high gamma oscillations (Colgin et al. 2009; Jackson et al. 2011; of course an oscillating common input is not strictly required if the receiving structure generates its own oscillations in response to input). Similarly,

the basolateral amygdala LFP exhibits gamma oscillations (although the sources of this have not been clearly shown; Popescu et al. 2009; Likhtik et al. 2014) and projects to vStr and mPFC (Shinonaga et al., 1994). Finally, the medial thalamus projects to both structures (Otake and Nakamura, 1998), although reports of gamma oscillations generated there are few (but see Minlebaev et al. 2011)

Could a single common source account for the result that both amplitude and phase relationships differ from zero with *opposite directions* for low and high gamma bands? If transmission from the putative common source to mPFC and vStr is homogeneous, the directionality reversal is a logical impossibility: for each frequency band, whichever recording site is closest to the common source would lead the other. Note that this is true even if volume conduction is associated with non-zero propagation speed (as found by e.g. Zhang et al. 2014) and/or the extracellular medium exhibits frequency-dependent capacitance in the gamma range. However, if conduction to both recording sites is *not* homogeneous (Bédard et al., 2004; Nelson et al., 2013), it is possible in principle that a specific inhomogeneity in the conductance of gamma-band frequencies combined with a common source, could account for the observed results. For instance, if low-gamma oscillations experienced slower conductance to mPFC than to vStr than high-gamma, something like the observed results could arise. However, such inhomogeneities are thought to be very small, if they exists at all within such a narrow frequency range (Ranck, 1963; Nicholson and Freeman, 1975; Logothetis et al., 2007; Kajikawa and Schroeder, 2015) thus we believe this possibility to be unlikely. Beyond a single common source, mixtures from two distinct sources (one for low-gamma and another for high-gamma) are possible in principle: a low-gamma source relatively closer to vStr and a separate, lower-amplitude high-gamma source relatively closer to mPFC, combined with a finite conduction speed, could produce the observed reversal. How this could be reconciled with the striking temporal precision with which low- and high-gamma seem to be coordinated (Dejean et al., 2013; Malhotra et al., 2015) would however remain unclear in such a scenario.

Next, it should be pointed out that the known conduction delays between mPFC and vStr (2-6 ms; Fino 2005; Bosch et al. 2012) seem to be incompatible with an asymmetric, one-area-driving-the-other scenario in which oscillations in one area (say vStr) are caused by inputs from an oscillating mPFC; this is the

main reason why we suggest the coupled oscillator interpretation as the more likely alternative. Of course the possibility of vStr driving mPFC this way would be less likely still, given the indirect nature of that projection. Finally, it is important to rule out technical reasons for the observed pattern of results. We tested our analysis workflow both with simulated data and with synthetic test signals in the low and high-gamma band fed into the recording system; these controls seem to rule out artifactual causes for the observed results.

Thus, in sum, we suggest that the observed temporal asymmetries between low- and high-gamma are unlikely to arise from a single common source; such explanations would require a highly specific inhomogeneity in volume conduction. Instead, this asymmetry may arise from transient deviations from a perfect coupling with zero phase lag, reflecting one area temporarily leading or lagging as a result of dynamically changing inputs and effective connectivity. Regardless of which interpretation ultimately proves correct, the issue of how the observed temporal asymmetry between low- and high-gamma comes is secondary to the main observation of near-zero lag synchrony between mPFC and vStr.

Functional relevance of gamma synchronization between mPFC and vStr

In general, gamma-band synchronization has been suggested as a possible mechanism for binding anatomically segregated features of a coherent cell assembly, as occurs for instance when encoding visual percepts (Tallon-Baudry, 1999; Engel and Singer, 2001). The functional significance of such synchronization is thought to stem from the increased effectiveness of such coordinated assemblies in activating common projection targets; in the case of mPFC and vStr those may include areas such as the ventral tegmental area (VTA; Haber 2009) and perhaps other basal ganglia nuclei such as the subthalamic nucleus (STN; Maurice et al. 1998).

A related but distinct proposal regarding the functional relevance of gamma-band synchronization is the "communication through coherence" hypothesis and its ongoing refinements (Singer, 1999; Fries, 2005;

Akam and Kullmann, 2014). This idea contends that circuits with anatomically fixed connectivity can nonetheless dynamically change their effective connectivity through inter-area synchronization of oscillatory activity. However, it is unclear if the very short time lags observed here, on the order of $\pm$ 1 ms in opposite directions from zero lag, would be sufficient to have a meaningful impact on the direction of information flow between mPFC and vStr. Interestingly, Chang et al. (2000) found that the spiking of pairs of neurons, simultaneously recorded in mPFC and vStr, commonly synchronize with zero time lag.

In any case, there is a substantial literature on the behavioral functions of the prefrontal-ventral striatal pathway, including disconnection studies in a variety of tasks (Christakou et al., 2004; Goto and Grace, 2008; Bossert et al., 2012) and identification of mPFC-vStr projection neurons as activated by motivationally relevant stimuli (McGinty and Grace, 2008; Britt et al., 2012). The question of whether gamma oscillations (or indeed, any oscillation) and their inter-area synchrony play a role in mediating these functions, provide a biomarker for joint activation without being causally important for anything, or are merely an epiphenomenon, is one currently being confronted in many neural systems. Our demonstration that ensemble spiking of vStr neurons can be used to classify the identity of the accompanying gamma oscillation (low- or high-gamma) suggests that at least, these oscillations are linked to spiking activity, and provides a basis for linking specific information content such as stimulus and outcome identities, value-related signals to these oscillations. Our results also inform the interpretation of an increasing number of studies aiming to translate limbic system LFP patterns from animal models to EEG/LFP recordings from human patient populations (McCracken and Grace, 2009; Uhlhaas and Singer, 2010; Donnelly et al., 2014).

Acknowledgments

We thank Jean Flanagan, Nancy Gibson and Martin Ryan for assistance with animal care and husbandry, and Alyssa Carey for technical assistance. This work was supported by NSERC, the National Science and Engineering Research Council of Canada (MvdM) and the Fondation FYSSEN (JC).

References

Adhikari, A., Sigurdsson, T., Topiwala, M. A., and Gordon, J. A. (2010). Cross-correlation of instantaneous amplitudes of field potential oscillations: a straightforward method to estimate the directionality and lag between brain areas. *Journal of neuroscience methods*, 191(2):191–200.

Akam, T. and Kullmann, D. M. (2014). Oscillatory multiplexing of population codes for selective communication in the mammalian brain. *Nature reviews. Neuroscience*, 15(2):111–22.

Alexander, G. E. and Crutcher, M. D. (1990). Functional architecture of basal ganglia circuits: neural substrates of parallel processing. *Trends Neurosci*, 13(7):266–271.

Bartos, M., Vida, I., and Jonas, P. (2007). Synaptic mechanisms of synchronized gamma oscillations in inhibitory interneuron networks. *Nature reviews. Neuroscience*, 8(1):45–56.

Bastos, A. M., Vezoli, J., and Fries, P. (2015). Communication through coherence with inter-areal delays. *Current Opinion in Neurobiology*, 31:173–180.

Bédard, C., Kröger, H., and Destexhe, A. (2004). Modeling extracellular field potentials and the frequency-filtering properties of extracellular space. *Biophysical journal*, 86(3):1829–42.

Berke, J. D. (2009). Fast oscillations in cortical-striatal networks switch frequency following rewarding events and stimulant drugs. *European Journal of Neuroscience*, 30(5):848–59.

Berke, J. D., Okatan, M., Skurski, J., and Eichenbaum, H. B. (2004). Oscillatory Entrainment of Striatal Neurons in Freely-Moving Rats. *Neuron*, 43(6):883–896.

Boraud, T., Brown, P., Goldberg, J. A., Graybiel, A. M., and Magill, P. J. (2002). Oscillations in the basal ganglia: The good, the bad, and the unexpected. *Neuropharmacology*, pages 3–24.

Bosch, C., Mailly, P., Degos, B., Deniau, J.-M., and Venance, L. (2012). Preservation of the hyperdirect pathway of basal ganglia in a rodent brain slice. *Neuroscience*, 215:31–41.

Bosman, C. A., Schoffelen, J.-M., Brunet, N., Oostenveld, R., Bastos, A. M., Womelsdorf, T., Rubehn, B., Stieglitz, T., De Weerd, P., and Fries, P. (2012). Attentional stimulus selection through selective synchronization between monkey visual areas. *Neuron*, 75(5):875–88.

Bossert, J. M., Stern, A. L., Theberge, F. R. M., Marchant, N. J., Wang, H.-L., Morales, M., and Shaham, Y. (2012). Role of projections from ventral medial prefrontal cortex to nucleus accumbens shell in context-induced reinstatement of heroin seeking. *The Journal of neuroscience : the official journal of the Society for Neuroscience*, 32(14):4982–91.

Britt, J., Benaliouad, F., McDevitt, R., Stuber, G., Wise, R., and Bonci, A. (2012). Synaptic and Behavioral Profile of Multiple Glutamatergic Inputs to the Nucleus Accumbens. *Neuron*, 76(4):790–803.

Buzsáki, G. (2006). *Rhythms of the Brain*. Oxford.

Buzsáki, G., Anastassiou, C. A., and Koch, C. (2012). The origin of extracellular fields and currents–EEG, ECoG, LFP and spikes. *Nature reviews. Neuroscience*, 13(6):407–20.

Buzsáki, G. and Schomburg, E. W. (2015). What does gamma coherence tell us about inter-regional neural communication? *Nature Neuroscience*, 18(4):484–9.

Buzsáki, G. and Wang, X.-J. (2012). Mechanisms of gamma oscillations. *Annual review of neuroscience*, 35:203–25.

Carmichael, J. and van der Meer, M. A. A. (2015). Unilateral naris occlusion abolishes gamma oscillations in the ventral striatum. *Society for Neuroscience Abstracts*.

Chang, J. Y., Janak, P. H., and Woodward, D. J. (2000). Neuronal and behavioral correlations in the medial prefrontal cortex and nucleus accumbens during cocaine self-administration by rats. *Neuroscience*, 99(3):433–43.

Christakou, A., Robbins, T. W., and Everitt, B. J. (2004). Prefrontal cortical-ventral striatal interactions involved in affective modulation of attentional performance: implications for corticostriatal circuit function. *The Journal of neuroscience : the official journal of the Society for Neuroscience*, 24(4):773–80.

Cohen, M. X., Bour, L., Mantione, M., Figee, M., Vink, M., Tijssen, M. A. J., van Rootselaar, A.-F., van den Munckhof, P., Schuurman, P. R., and Denys, D. (2012). Top-down-directed synchrony from medial frontal cortex to nucleus accumbens during reward anticipation. *Human brain mapping*, 33(1):246–52.

Colgin, L. L., Denninger, T., Fyhn, M., Hafting, T., Bonnevie, T., Jensen, O., Moser, M.-B., and Moser, E. I. (2009). Frequency of gamma oscillations routes flow of information in the hippocampus. *Nature*, 462(7271):353–357.

Courtemanche, R., Fujii, N., and Graybiel, A. M. (2003). Synchronous, focally modulated beta-band oscillations characterize local field potential activity in the striatum of awake behaving monkeys. *Journal of Neuroscience*, 23(37):11741–52.

Cruz, A. V., Mallet, N., Magill, P. J., Brown, P., and Averbeck, B. B. (2011). Effects of dopamine depletion on information flow between the subthalamic nucleus and external globus pallidus. *Journal of neurophysiology*, 106(4):2012–23.

Dejean, C., Arbuthnott, G., Wickens, J. R., Le Moine, C., Boraud, T., and Hyland, B. I. (2011). Power fluctuations in beta and gamma frequencies in rat globus pallidus: association with specific phases of slow oscillations and differential modulation by dopamine D1 and D2 receptors. *Journal of Neuroscience*, 31(16):6098–107.

Dejean, C., Boraud, T., and Le Moine, C. (2013). Opiate dependence induces network state shifts in the limbic system. *Neurobiology of disease*, 59:220–9.

Dejean, C., Nadjar, A., Le Moine, C., Bioulac, B., Gross, C. E., and Boraud, T. (2012). Evolution of the dynamic properties of the cortex-basal ganglia network after dopaminergic depletion in rats. *Neurobiology of disease*, 46(2):402–13.

Donnelly, N. A., Holtzman, T., Rich, P. D., Nevado-Holgado, A. J., Fernando, A. B. P., Van Dijck, G., Holzhammer, T., Paul, O., Ruther, P., Paulsen, O., Robbins, T. W., and Dalley, J. W. (2014). Oscillatory Activity in the Medial Prefrontal Cortex and Nucleus Accumbens Correlates with Impulsivity and Reward Outcome. *PloS one*, 9(10):e111300.

Engel, A. K. and Singer, W. (2001). Temporal binding and the neural correlates of sensory awareness. *Trends in Cognitive Sciences*, 5(1):16–25.

583 Fino, E. (2005). Bidirectional Activity-Dependent Plasticity at Corticostriatal Synapses. *Journal of Neuroscience*, 25(49):11279–
584 11287.

585 Fries, P. (2005). A mechanism for cognitive dynamics: neuronal communication through neuronal coherence. *Trends in Cognitive*
586 *Sciences*, 9(10):474–80.

587 Fries, P., Nikolič, D., and Singer, W. (2007). The gamma cycle. *Trends Neurosci*, 30(7):309–316.

588 Friston, K. J., Bastos, A. M., Pinotsis, D., and Litvak, V. (2014). LFP and oscillations-what do they tell us? *Current opinion in*
589 *neurobiology*, 31C:1–6.

590 Gollo, L. L., Mirasso, C., Sporns, O., and Breakspear, M. (2014). Mechanisms of zero-lag synchronization in cortical motifs. *PLoS*
591 *computational biology*, 10(4):e1003548.

592 Goto, Y. and Grace, A. A. (2008). Limbic and cortical information processing in the nucleus accumbens. *Trends in neurosciences*,
593 31(11):552–8.

594 Groenewegen, H., der Zee, E., Te Kortschot, A., and Witter, M. (1987). Organization of the projections from the subiculum to the
595 ventral striatum in the rat. A study using anterograde transport of Phaseolus vulgaris leucoagglutinin. *Neuroscience*, 23(1):103–
596 120.

597 Gruber, A. J., Hussain, R. J., and O'Donnell, P. (2009). The Nucleus Accumbens: A Switchboard for Goal-Directed Behaviors.
598 *PLoS ONE*, 4(4):e5062.

599 Haber, S. N. (2009). Anatomy and connectivity of the reward circuit. In Dreher, J.-C. and Tremblay, L., editors, *Handbook of*
600 *Reward and Decision Making*, pages 3–27. Academic Press.

601 Haber, S. N., Fudge, J. L., and McFarland, N. R. (2000). Striatonigrostriatal pathways in primates form an ascending spiral from the
602 shell to the dorsolateral striatum. *The Journal of neuroscience : the official journal of the Society for Neuroscience*, 20(6):2369–
603 82.

604 Hammond, C., Bergman, H., and Brown, P. (2007). Pathological synchronization in Parkinson's disease: networks, models and
605 treatments. *Trends Neurosci*, 30(7):357–364.

606 Howe, M. W., Atallah, H. E., McCool, A., Gibson, D. J., and Graybiel, A. M. (2011). Habit learning is associated with major shifts
607 in frequencies of oscillatory activity and synchronized spike firing in striatum. *Proceedings of the National Academy of Sciences*,
608 108(40):16801–6.

609 Humphries, M. and Prescott, T. (2010). The ventral basal ganglia, a selection mechanism at the crossroads of space, strategy, and
610 reward. *Progress in Neurobiology*, 90(4):385–417.

611 Jackson, J., Goutagny, R., and Williams, S. (2011). Fast and Slow Gamma Rhythms Are Intrinsically and Independently Generated
612 in the Subiculum. *Journal of Neuroscience*, 31(34):12104–12117.

613 Jay, T. M. and Witter, M. P. (1991). Distribution of hippocampal CA1 and subicular efferents in the prefrontal cortex of the rat studied
614 by means of anterograde transport of Phaseolus vulgaris-leucoagglutinin. *The Journal of comparative neurology*, 313(4):574–86.

615 Kajikawa, Y. and Schroeder, C. E. (2015). Generation of field potentials and modulation of their dynamics through volume integra-
616 tion of cortical activity. *Journal of neurophysiology*, 113(1):339–51.

617 Kalenscher, T., Lansink, C. S., Lankelma, J. V., and Pennartz, C. M. A. (2010). Reward-associated gamma oscillations in ventral
618 striatum are regionally differentiated and modulate local firing activity. *Journal of Neurophysiology*, 103(3):1658–72.

619 Koralek, A., Costa, R., and Carmena, J. (2013). Temporally Precise Cell-Specific Coherence Develops in Corticostriatal Networks
620 during Learning. *Neuron*.

621 Lemaire, N., Hernandez, L. F., Hu, D., Kubota, Y., Howe, M. W., and Graybiel, A. M. (2012). Effects of dopamine depletion on
622 LFP oscillations in striatum are task- and learning-dependent and selectively reversed by L-DOPA. *Proceedings of the National*
623 *Academy of Sciences of the United States of America*, 109(44):18126–31.

624 Leventhal, D. K., Gage, G. J., Schmidt, R., Pettibone, J. R., Case, A. C., and Berke, J. D. (2012). Basal Ganglia Beta oscillations
625 accompany cue utilization. *Neuron*, 73(3):523–36.

626 Likhtik, E., Stujenske, J. M., Topiwala, M. A., Harris, A. Z., and Gordon, J. A. (2014). Prefrontal entrainment of amygdala activity
627 signals safety in learned fear and innate anxiety. *Nature neuroscience*, 17(1):106–13.

628 Lisman, J. E. and Jensen, O. (2013). The θ-γ neural code. *Neuron*, 77(6):1002–16.

629 Logothetis, N. K., Kayser, C., and Oeltermann, A. (2007). In vivo measurement of cortical impedance spectrum in monkeys:
630 implications for signal propagation. *Neuron*, 55(5):809–23.

631 Malhotra, S., Cross, R. W., Zhang, A., and van der Meer, M. A. A. (2015). Ventral striatal gamma oscillations are highly vari-
632 able from trial to trial, dominated by behavioral state, and only weakly influenced by outcome value. *European Journal of*
633 *Neuroscience*, in press.

634 Maurice, N., Deniau, J. M., Glowinski, J., and Thierry, A. M. (1998). Relationships between the prefrontal cortex and the basal
635 ganglia in the rat: physiology of the corticosubthalamic circuits. *The Journal of neuroscience : the official journal of the Society*
636 *for Neuroscience*, 18(22):9539–46.

637 McCracken, C. B. and Grace, A. A. (2009). Nucleus accumbens deep brain stimulation produces region-specific alterations in local
638 field potential oscillations and evoked responses in vivo. *The Journal of neuroscience : the official journal of the Society for*
639 *Neuroscience*, 29(16):5354–63.

640 McGinty, V. B. and Grace, A. A. (2008). Selective activation of medial prefrontal-to-accumbens projection neurons by amygdala
641 stimulation and Pavlovian conditioned stimuli. *Cerebral cortex (New York, N.Y. : 1991)*, 18(8):1961–72.

642 Minlebaev, M., Colonnese, M., Tsintsadze, T., Sirota, A., and Khazipov, R. (2011). Early γ oscillations synchronize developing
643 thalamus and cortex. *Science*, 334(6053):226–9.

644 Mitzdorf, U. (1985). Current source-density method and application in cat cerebral cortex: investigation of evoked potentials and
645 EEG phenomena. *Physiological reviews*, 65(1):37–100.

646 Morra, J. T., Glick, S. D., and Cheer, J. F. (2012). Cannabinoid receptors mediate methamphetamine induction of high frequency
647 gamma oscillations in the nucleus accumbens. *Neuropharmacology*, 63(4):565–74.

Nelson, M. J., Bosch, C., Venance, L., and Pouget, P. (2013). Microscale inhomogeneity of brain tissue distorts electrical signal propagation. *Journal of Neuroscience*, 33(7):2821–7.

Nicholson, C. and Freeman, J. A. (1975). Theory of current source-density analysis and determination of conductivity tensor for anuran cerebellum. *J Neurophysiol*, 38(2):356–368.

Nolte, G., Ziehe, A., Nikulin, V., Schlögl, A., Krämer, N., Brismar, T., and Müller, K.-R. (2008). Robustly Estimating the Flow Direction of Information in Complex Physical Systems. *Physical Review Letters*, 100(23):234101.

Nunez, P. L. and Srinivasan, R. (2006). *Electric Fields of the Brain: The Neurophysics of EEG*, volume 4. Oxford University Press.

Oostenveld, R., Fries, P., Maris, E., and Schoffelen, J.-M. (2011). FieldTrip: Open source software for advanced analysis of MEG, EEG, and invasive electrophysiological data. *Computational intelligence and neuroscience*, 2011:156869.

Otake, K. and Nakamura, Y. (1998). Single midline thalamic neurons projecting to both the ventral striatum and the prefrontal cortex in the rat. *Neuroscience*, 86(2):635–49.

Pennartz, C. M. A., Berke, J. D., Graybiel, A. M., Ito, R., Lansink, C. S., van der Meer, M. A. A., Redish, A. D., Smith, K. S., and Voorn, P. (2009). Corticostriatal Interactions during Learning, Memory Processing, and Decision Making. *The Journal of Neuroscience*, 29(41):12831–8.

Popescu, A. T., Popa, D., and Paré, D. (2009). Coherent gamma oscillations couple the amygdala and striatum during learning. *Nature neuroscience*, 12(6):801–7.

Ranck, J. B. (1963). Analysis of specific impedance of rabbit cerebral cortex. *Experimental Neurology*, 7(2):153–174.

Sesack, S. R. and Grace, A. A. (2010). Cortico-Basal Ganglia reward network: microcircuitry. *Neuropsychopharmacology*, 35(1):27–47.

Sharott, A., Moll, C. K. E., Engler, G., Denker, M., Grün, S., and Engel, A. K. (2009). Different subtypes of striatal neurons are selectively modulated by cortical oscillations. *The Journal of neuroscience : the official journal of the Society for Neuroscience*, 29(14):4571–85.

Shinonaga, Y., Takada, M., and Mizuno, N. (1994). Topographic organization of collateral projections from the basolateral amygdaloid nucleus to both the prefrontal cortex and nucleus accumbens in the rat. *Neuroscience*, 58(2):389–97.

Singer, W. (1999). Neuronal synchrony: a versatile code for the definition of relations? *Neuron*, 24(1):49–65,111–125.

Stujenske, J., Likhtik, E., Topiwala, M., and Gordon, J. (2014). Fear and Safety Engage Competing Patterns of Theta-Gamma Coupling in the Basolateral Amygdala. *Neuron*, 83(4):919–933.

Tallon-Baudry, C. (1999). Oscillatory gamma activity in humans and its role in object representation. *Trends in Cognitive Sciences*, 3(4):151–162.

Thorn, C. A. and Graybiel, A. M. (2014). Differential entrainment and learning-related dynamics of spike and local field potential activity in the sensorimotor and associative striatum. *Journal of Neuroscience*, 34(8):2845–59.

Traub, R. D., Whittington, M. A., Stanford, I. M., and Jefferys, J. G. (1996). A mechanism for generation of long-range synchronous

fast oscillations in the cortex. *Nature*, 383(6601):621–4.

Uhlhaas, P. J., Pipa, G., Lima, B., Melloni, L., Neuenschwander, S., Nikolič, D., and Singer, W. (2009). Neural synchrony in cortical networks: history, concept and current status. *Front Integr Neurosci*, 3:17.

Uhlhaas, P. J. and Singer, W. (2010). Abnormal neural oscillations and synchrony in schizophrenia. *Nature reviews. Neuroscience*, 11(2):100–13.

van der Meer, M. A. A., Kalenscher, T., Lansink, C. S., Pennartz, C. M. A., Berke, J. D., and Redish, A. D. (2010). Integrating early results on ventral striatal gamma oscillations in the rat. *Frontiers in Neuroscience*, 4:28.

van der Meer, M. A. A. and Redish, A. D. (2009a). Covert Expectation-of-Reward in Rat Ventral Striatum at Decision Points. *Frontiers in Integrative Neuroscience*, 3:1.

van der Meer, M. A. A. and Redish, A. D. (2009b). Low and High Gamma Oscillations in Rat Ventral Striatum have Distinct Relationships to Behavior, Reward, and Spiking Activity on a Learned Spatial Decision Task. *Frontiers in Integrative Neuroscience*, 3:9.

Vicente, R., Gollo, L. L., Mirasso, C. R., Fischer, I., and Pipa, G. (2008). Dynamical relaying can yield zero time lag neuronal synchrony despite long conduction delays. *Proceedings of the National Academy of Sciences of the United States of America*, 105(44):17157–62.

von Nicolai, C., Engler, G., Sharott, A., Engel, A. K., Moll, C. K., and Siegel, M. (2014). Corticostriatal coordination through coherent phase-amplitude coupling. *Journal of Neuroscience*, 34(17):5938–48.

Voorn, P., Vanderschuren, L. J., Groenewegen, H. J., Robbins, T. W., and Pennartz, C. M. (2004). Putting a spin on the dorsal-ventral divide of the striatum. *Trends in Neuroscience*, 27:468–474.

Womelsdorf, T., Valiante, T. A., Sahin, N. T., Miller, K. J., and Tiesinga, P. (2014). Dynamic circuit motifs underlying rhythmic gain control, gating and integration. *Nature neuroscience*, 17(8):1031–9.

Zhang, M., Ladas, T. P., Qiu, C., Shivacharan, R. S., Gonzalez-Reyes, L. E., and Durand, D. M. (2014). Propagation of epileptiform activity can be independent of synaptic transmission, gap junctions, or diffusion and is consistent with electrical field transmission. *The Journal of neuroscience : the official journal of the Society for Neuroscience*, 34(4):1409–19.

List of Figures

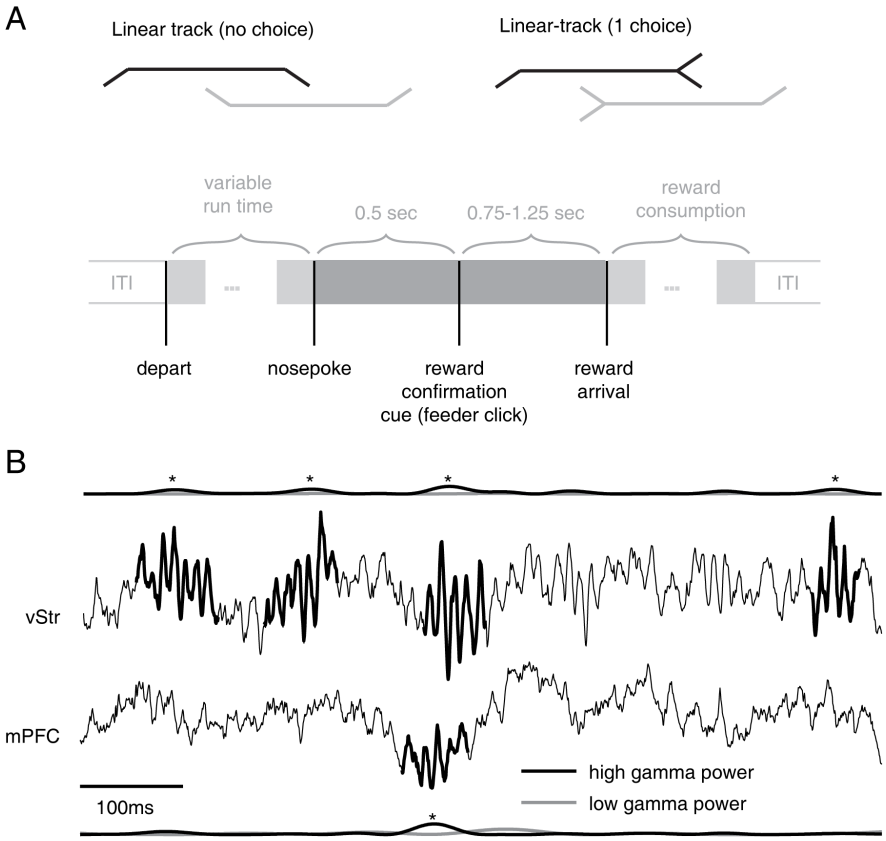

Figure 1: Task design and example local field potential traces. **A**: Layout of the behavioral apparatus used, an elevated linear track without (top left) or with (right) a choice point. Rats experienced one configuration per daily 40-minute recording session, starting on the no-choice track before advancing to the choice configuration. Each track configuration was pseudorandomized between days (with the alternate configurations shown in gray) such that there was no systematic association between body turns at the end of the track and reward. Food pellet rewards were dispensed at both ends of the track once the rat nosepoked into the reward receptacle for 700ms (bottom), with a further 800ms elapsing until rats made contact with the first food pellet. In the choice task, only one location was rewarded, and subject to reversal whenever 40 trials were performed with $\geq$90% correct in the last 20 trials. Because no differences between task conditions were found in the local field potential data, analyses collapsed across all task conditions. **B**: Example of simultaneously recorded local field potential signals from the ventral striatum (vStr) and medial prefrontal cortex (mPFC) during the task. Signal power in the low-gamma (45-65 Hz, gray) and high-gamma (70-90 Hz, black) is also shown, with stars indicating detected gamma events as determined by crossing a threshold (95th percentile; see *Methods*). Event times are highlighted by the bold traces in the LFPs, illustrating the tendency for mPFC gamma to occur synchronously with mPFC gamma.

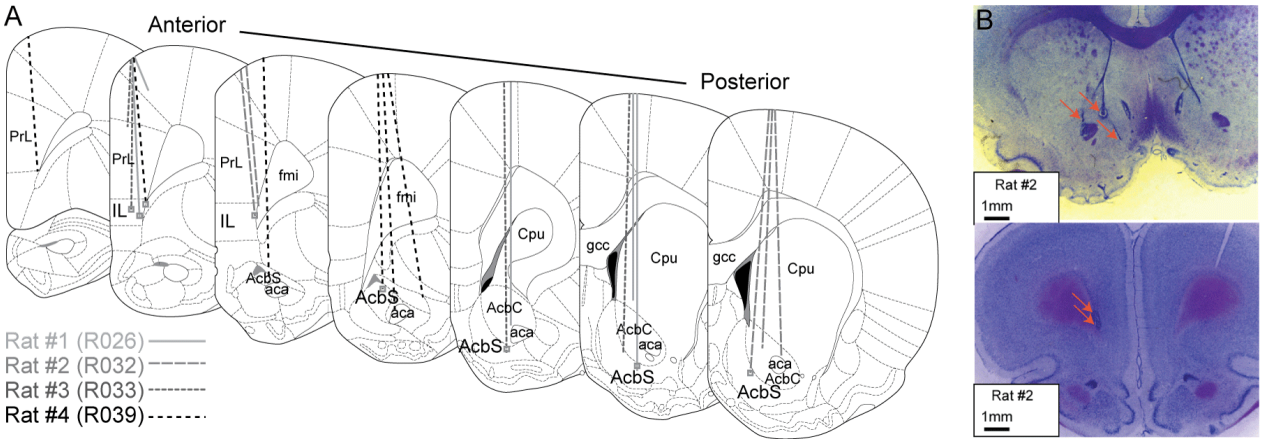

Figure 2: Verification of electrode locations in the ventral prelimbic (PrL) and infralimbic (IL) areas of the medial prefrontal cortex, and the nucleus accumbens core and shell (AcbC, AcbS). **A**: Schematic of electrode tracks for each subject, as determined by microscopy analysis of sectioned and stained brain tissue (**B**). Dashed lines indicate electrode tracks; tracks ending in a square marker were chosen for analysis. Electrodes were not advanced after recording commenced.

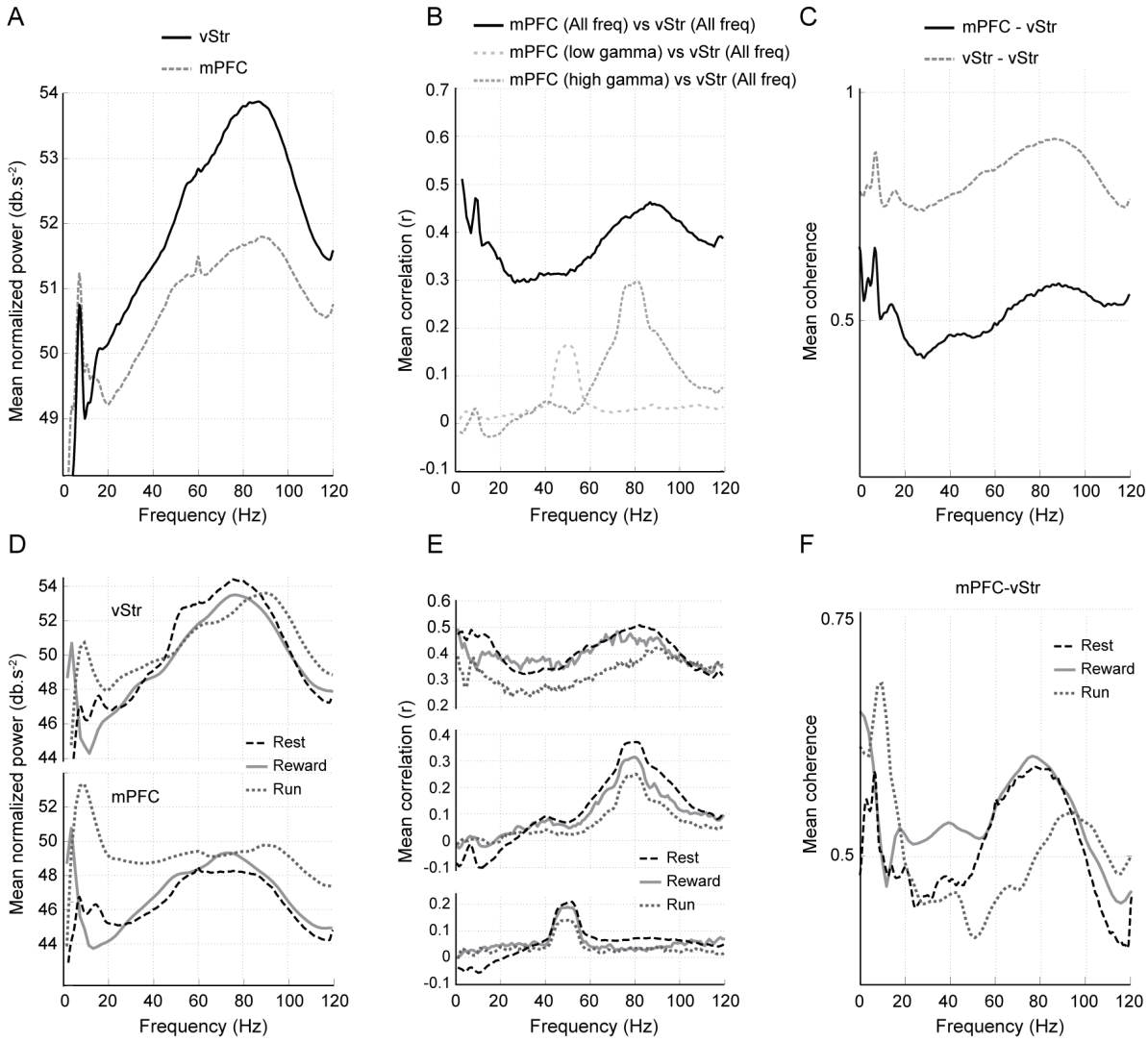

Figure 3: Phase and amplitude correlations between vStr and mPFC local field potentials. **A**: Power spectrum density (PSD) for vStr (black solid line) and mPFC (gray dashed line) normalized ($1/f^2$) and averaged over 8 sessions (4 rats); showing that the power in the gamma band was higher than the $1/f$ baseline. **B**: Power correlation (average) between vStr and mPFC. The cross-frequency correlation matrix diagonal band (black) shows high correlation values in the gamma bands; indicating that gamma oscillations tend to occur at similar time across the two structures. Each of the two horizontal bands (light gray: 45-65 Hz, dark gray: 70-90 Hz) show specific correlation increases with the corresponding frequency band in the other structure; indicating that a given gamma type tends to co-occur in mPFC and vStr. **C**: Coherence spectra (average) between mPFC-vStr (black) and vStr-vStr (dashed gray) show high coherence in the gamma band; indicating that gamma oscillations have a consistent phase relationship between the two recorded sites. **D**-F: As A-C, but for different behavioral epochs: running and reward periods on the task, and off-task rest periods. Note that gamma synchrony between structures is preserved.

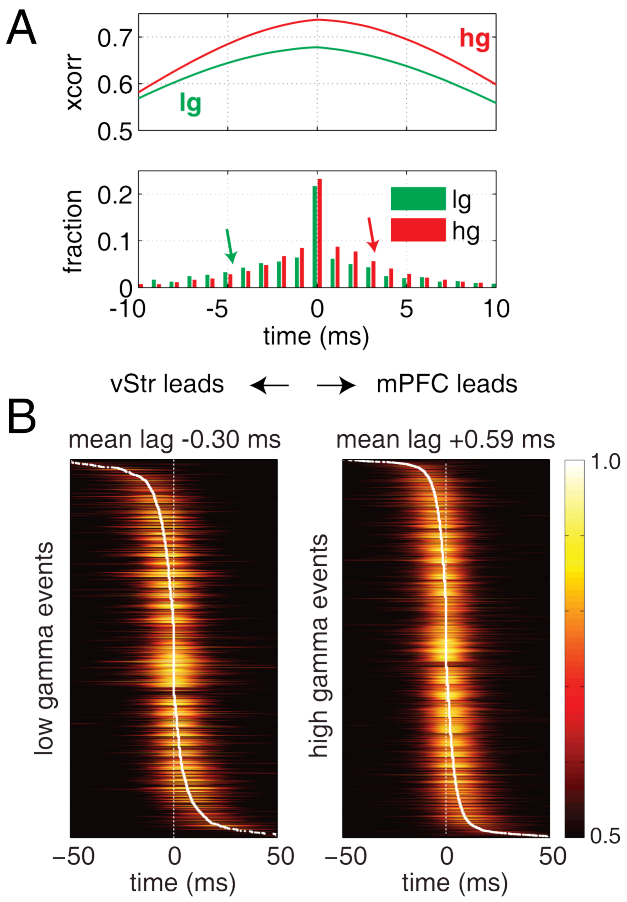

Figure 4: Power cross-correlations between vStr and mPFC reveal asymmetries between low and high-gamma oscillations. **A**: Average cross-correlation between vStr and mPFC (top) for detected low-gamma events (red) and high-gamma events (blue) and histogram of cross-correlation peaks (bottom). Note the asymmetry between the two distributions, indicated by the green arrow highlighting relatively more low gamma cross-correlation peaks on the vStr-lead side, and the red arrow indicating relatively more high-gamma peaks on the mPFC-lead side. **B**: Full distributions of cross-correlations for low-gamma (left) and high-gamma (right) events. Color scale indicates the correlation coefficient across time lags; white dots show the time of the peak cross-correlation for each events. Events are ordered according to this time, and the resulting distributions of peak times are shifted from zero in opposite directions for low-gamma (vStr lead, left direction), and high-gamma (mPFC lead, right direction).

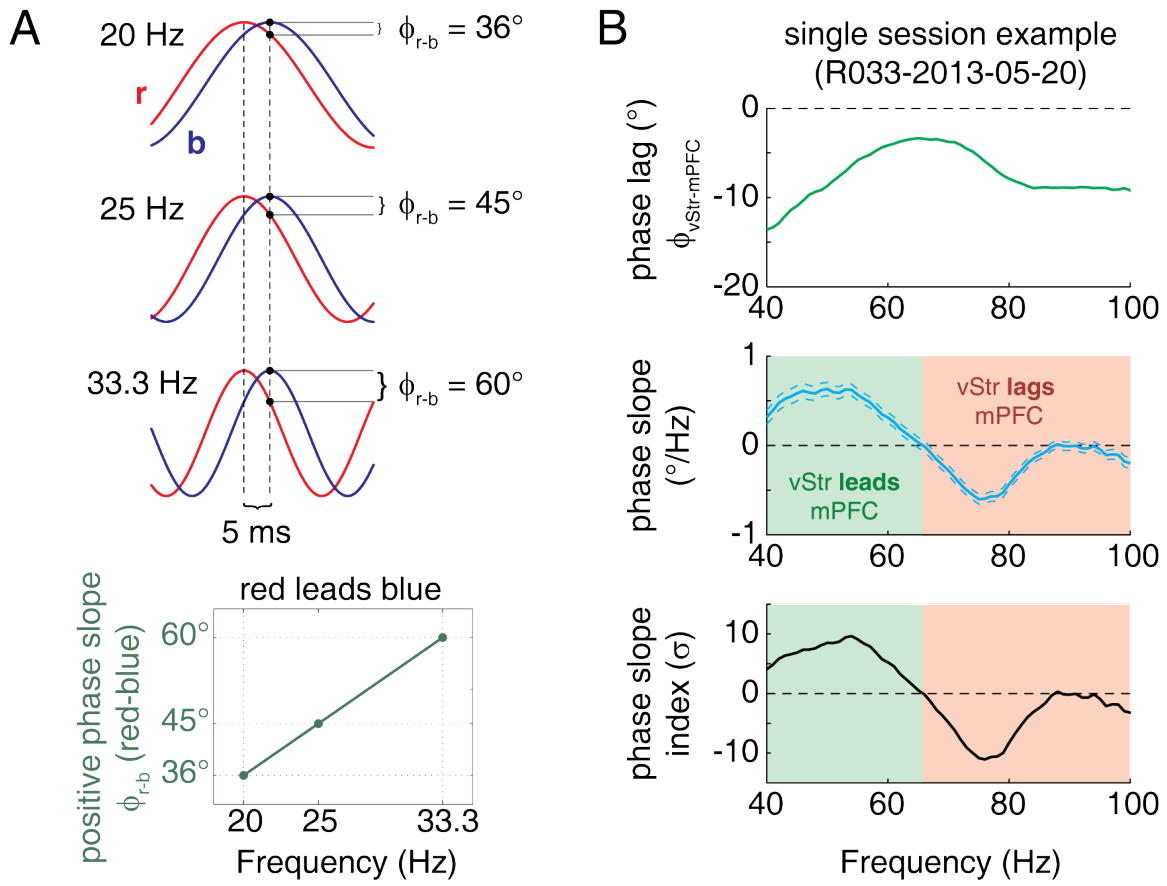

Figure 5: Schematic of the rationale underlying phase slopes, and computation of the phase slope index for an example recording session. **A**: Schematic of the linear relationship between phase lag and frequency used to interpret the phase slope. In this example, the red signal always leads the blue signal by 5 ms, which results in a different phase lag across frequencies (20, 25 and 33.3 Hz in this example). The bottom panel shows the linear relationship between phase lag and frequency for the above examples, resulting a positive slope for the red-blue phase difference indicating a red lead (green phase slope). **B**: Phase lags, phase slope, and phase slope index (PSI) for a single example "Task" session. Note that the phase lag as a function of frequency (top panel) contains approximately linear regions in the low-gamma (45-65 Hz, green) and high-gamma (70-90 Hz, red) frequency bands, with slopes in opposite directions. Phase lags are computed relative to vStr phase, so a negative phase lag indicates earlier phase in vStr compared to mPFC. The phase slope (middle panel) is the derivative of the raw phase lag, and the reversal of the phase slope sign around 65-70 Hz indicates that high and low gamma are associated with opposite directionality in the vStr-mPFC system, with vStr leading for low gamma and mPFC leading for high gamma oscillations. The bottom panel shows the phase slope index (PSI) which normalizes the raw phase slope by its standard deviation, obtained using a bootstrap (FieldTrip `ft_connectivityanalysis()` function).

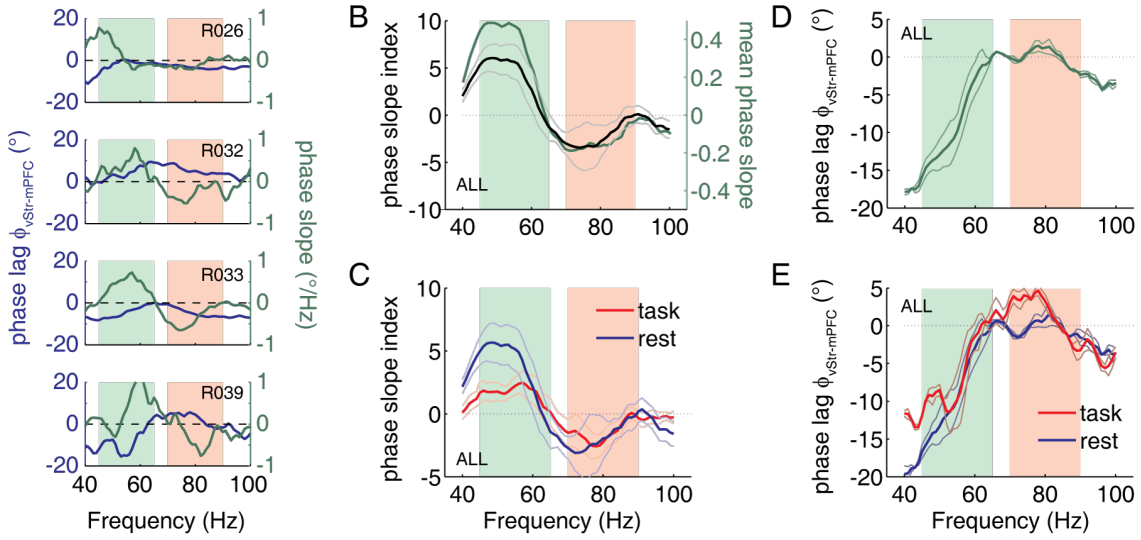

Figure 6: **A**: The phase slope reversal for low and high gamma is robust across subjects. Each example (one per rat) shows the phase lag (blue) and its derivative, the phase slope (green) across frequency, calculated over all gamma events. **B**: Phase slope index (PSI) and phase slope (green) as a function of frequency, averaged over all sessions (S.E.M. in dashed lines), similarly indicates that vStr leads during low-gamma and mPFC leads during high-gamma oscillations. **C**: The phase slope index reverses between low and high gamma during both task (red) and rest (blue) epochs (averages over 8 sessions). There is a slight overall shift in frequency between rest and task (also seen in the power spectra, see Figure 3D) but the PSI reversal between low and high-gamma is preserved. Light green and light red shading indicate the low-gamma band (45-65Hz) and high-gamma band (70-90Hz) respectively. **D**: Average phase lag across sessions for all data similarly shows a systematic shift as a function of gamma band frequency, particularly evident during task performance (**E**). As in Figure 5, phase lags are computed relative to vStr phase such that a negative phase lag indicates earlier phase in vStr compared to mPFC; conversely, positive phase lag indicates earlier phase in mPFC compared to vStr. Note that these absolute phase differences should be interepreted with caution due to their inherent circularity and dependence on precise electrode location relative to currrent sinks and sources.

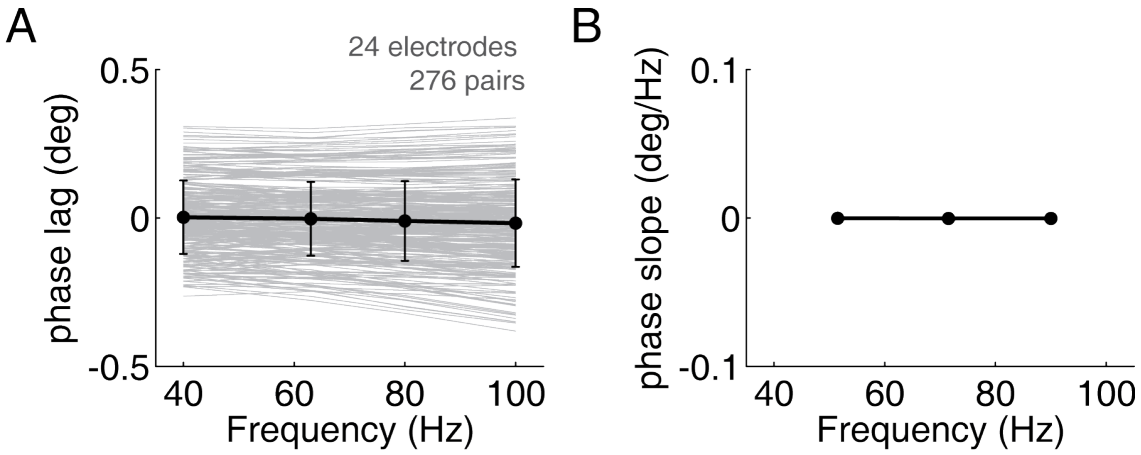

Figure 7: Electrode and recording system properties cannot account for the observed phase lags. **A**: Observed phase lags as a function of frequency for 276 electrode pairs (each line corresponds to one pair) when presented with sinusoidal test signals at 40, 63, 80 and 100 Hz. The magnitude of the phase lags to these artificial signals is much smaller than those observed for mPFC and vStr LFPs (compare Figure 6A) and although there were main effects of frequency and electrode impedance on the phase lag, there was no evidence of interaction between them (ANOVA, see main text). **B**: Average phase slopes over the frequencies shown in A are effectively zero, unlike in the neural data; compare Figure 6A.

Figure 8: Schematic illustrating the classification of gamma events based on ensemble spiking activity. A linear discriminant classifier was trained to associate spike counts from ensembles of simultaneously recorded ventral striatal neurons with low-gamma (lg, green) or high-gamma (hg, red) events. Classifier performance was tested on events not included in the training set (black dashed lines, "?") and compared to a control condition in which labels were associated with time-shifted events of equivalent length.

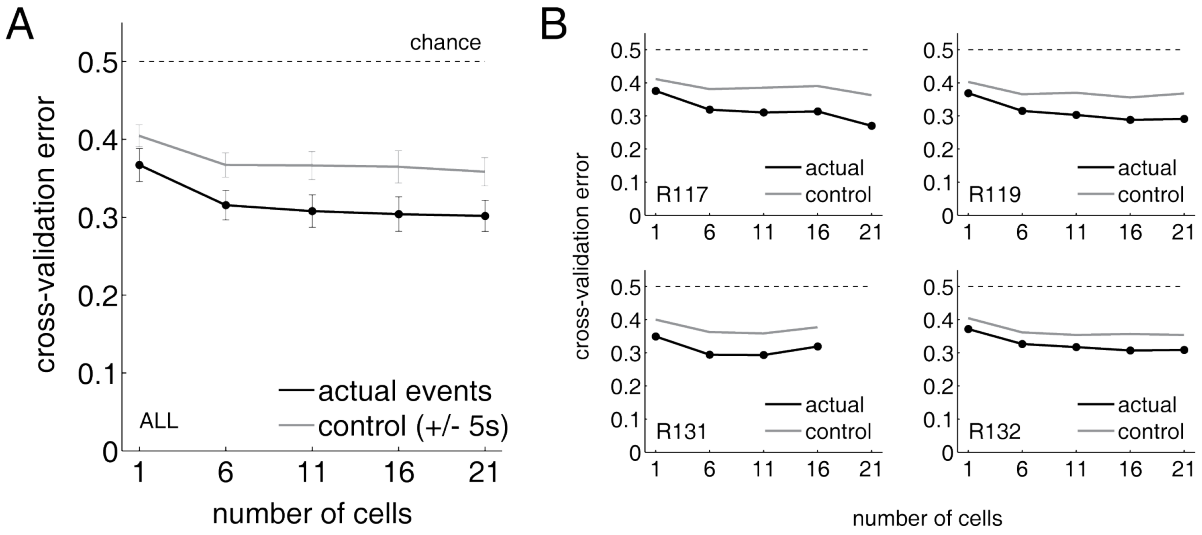

Figure 9: Low- and high-gamma events in the ventral striatal local field potential (LFP) are associated with distinct neural ensembles. **A**: Proportion of classification errors in associating ensemble spiking with low- or high-gamma LFP events relative the chance level (0.5; 0 indicates perfect classification) as a function of ensemble size. Performance of the linear discriminant classifier on testing data under 10-fold cross-validation (for the best performing ensemble of the given size) is shown in continuous black for the original data; in dashed light gray for the control condition (spike data shifted by up to 5 s relative to the LFP). These results indicate an association between each gamma oscillation type and a distinct pattern of activation at the ensemble level. **B**: As in panel A, but for individual subjects, showing that the pattern of results is robust.